

Supplementary Information

Realizing Room Temperature Catalytic Hydrogenation of Sodium Phenoxide by Ru/TiO₂ for Hydrogen Storage

#Khai Chen Tan,^{abc} #Qijun Pei,^a Jiafeng Yu,^a Hong Wen,^a Yang Yu,^a Jintao Wang,^{ab} Nor Izzati Nordin,^c Teng He,^{*ab} Yong Shen Chua,^{*c} and Ping Chen^{ab}

^a Dalian Institute of Chemical Physics, Chinese Academy of Sciences, Dalian, 116023, China.

^b Centre of Material Science and Optoelectronics Engineering, University of Chinese Academy of Sciences, Beijing 100049, China.

^c School of Chemical Sciences, Universiti Sains Malaysia, 11800 Minden, Penang, Malaysia.

*Corresponding authors.

E-mail addresses:

heteng@dicp.ac.cn (T. He)

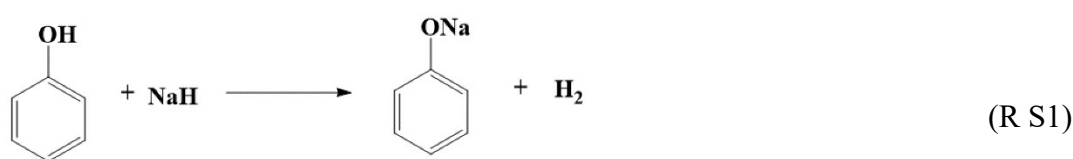
yschua@usm.my (Y. S. Chua)

#K.C. Tan and Q. Pei contributed equally to this work.

Experimental Section

1.1. Material Syntheses

Phenol (Fisher, $\geq 99\%$), sodium hydride (Aldrich, 90%), ruthenium (III) chloride hydrate (ACROS, 35–40% Ru), platinum acetylacetonate (Merck, 50% Pt), palladium (II) acetate (Merck, 47% Pd), sodium borohydride (Aldrich), ruthenium on alumina (Aldrich, 5.0% Ru), titanium (IV) oxide (Aldrich, P25 $\geq 99.5\%$), and hydrogen gas (Air Products, 99.9992%) were commercially available and used as received without further purification. Molecular sieves were added to the dimethyl sulfoxide- d_6 (Aldrich, 99.9 atom % D) to remove the moisture. Sodium phenoxide was synthesized following the procedure as reported elsewhere¹. Typically, 0.1 mol of phenol and 0.11 mol of sodium hydride was put into a 94.1 mL stainless steel and ball-milled for 8 h at 200 rpm with the ball to sample mass ratio of 100:1. The pressure accumulated in ball milling vessel was monitored by pressure gauge, and *ca.* 1.0 equivalent mol H_2 was liberated after ball-milling, indicating the formation of sodium phenoxide occurred via reaction (R S1). Because sodium hydride is moisture and air sensitive, therefore the synthesis of sodium phenoxide was conducted in a glovebox filled with high purity of argon.



1.2 Catalyst Syntheses

Different amount of Ru (2.0%, 5.0%, and 9.7%) were doped onto TiO_2 using a wet impregnation approach. In brief, metal loading was achieved by impregnating TiO_2 with an aqueous solution of $RuCl_3$ at a specific concentration. The mixture was stirred for 5 h prior to the reduction process. $NaBH_4$ solution was added dropwise to reduce the Ru^{3+} cations with vigorous stirring. The end-product was then filtered, washed with distilled water and dried under vacuum overnight. The same protocols were repeated, except that platinum

acetylacetonate and palladium (II) acetate were utilised as precursors to prepare 5.0% Pt/TiO₂ and 5.0% Pd/TiO₂, respectively.

1.3 Catalytic Hydrogenation

In a typical hydrogenation reaction experiment, 0.5 mmol of sodium phenoxide was grinded with 5.0% Ru/TiO₂ (101 mg) catalyst at sodium phenoxide:Ru molar ratio of 1:10. The mixture was then loaded into a vessel (207 mL), sealed and heated to desired temperatures at a heating rate of 2 °C min⁻¹. Once the desired temperature has been reached, 20 bar of H₂ was introduced into the vessel. After a set period of time, the vessel was allowed to cool down to room temperature and the remaining hydrogen was discharged. The same procedures were repeated using 2.0% Ru/TiO₂ (252 mg), 9.7% Ru/TiO₂ (52 mg), 5.0% Pd/TiO₂ (106 mg), 5.0% Pt/TiO₂ (195 mg), and 5.0% Ru/Al₂O₃ (101 mg) as catalysts, respectively. Besides, the activities of hydrogenation at different parameters (pressure, temperature, Ru-loading content, and reaction time) were also studied for comparison. The catalytic hydrogenation conversions and selectivity towards sodium cyclohexanolate were quantified by ¹H Nuclear Magnetic Resonance (NMR).

1.4 Characterizations

Liquid ¹H NMR spectroscopy was conducted on a Bruker AVANCE 500 MHz NMR spectrometer (11.7 T) at ambient temperature with DMSO as the deuterated solvent. X-ray diffraction (XRD) measurements were carried out on a Bruker D8 Advance (Cu-K α radiation, $\lambda=0.154$ nm; 40 kV; 40 mA). The X-ray photoelectron spectroscopy (XPS) measurements were performed by K-Alpha X-ray photoelectron spectrometer (Thermo Fisher Scientific) using a monochromatic Al K α radiation (photon energy = 1486.6 eV). With an X-ray spot size of 400 μ m and pass energies of 100 eV for wide scan and 30 eV for individual elements, spectra were acquired from 0 to 1350 eV. The binding energy was calibrated relative to the C 1s peak at 284.8 eV². Transmission electron microscopy (TEM) images were collected on a

FEI Talos F200S microscope operating at 200 kV. Carbon monoxide-diffuse reflectance infrared Fourier transform spectroscopy (CO-DRIFTS) measurements were carried out on a TENSOR II infrared spectrometer (Bruker), in diffuse reflectance mode, equipped with a mercury cadmium telluride (MCT) detector. The 5.0% Ru/Al₂O₃ catalyst was reduced at 250 °C. The sample crucible was filled with a flat sample, and was purged with Ar for 10 min to obtain a background spectrum. Then, 5% CO/Ar gas (flow rate of 30 mL min⁻¹) was introduced. Prior to measuring the absorbance spectrum, the latter was shifted to Ar purging (flow rate 30 mL min⁻¹) for an additional 10 min to eliminate the CO gas in the sample holder. The CO-DRIFTS spectrum was then obtained. X-ray absorption fine structure (XAFS) experiments at Ru K edge (22,117 eV) were performed at the BL14W1 beamline of the Shanghai Synchrotron Radiation Facility (SSRF) using a Si (311) double-crystal monochromator. To prevent contamination of air prior to the test, the samples were sealed with KAPTON film. The spectra were recorded in transmission mode at room temperature, and the energy was calibrated using Ru foil. All of the data were processed and analyzed using the IFFEFIT software package³. Spectra were k^3 -weighted and fitted in the range of $R = 1.0$ - 2.8 Å and $k = 3.0$ - 14.0 Å⁻¹. The amplitude reduction factor (S_0^2), as determined from Ru foil, was fixed at 0.733. The coordination numbers (CN), energy shift parameter (δE_0), the bond lengths (Distance) and Debye-Waller factors (σ^2) were fitted as guess parameters. Standard metallic Ru model: Ru–Ru with CN=6 at 2.677 Å and CN=6 at 2.724 Å.

1.5 Calculation

The geometries were optimized at the B3LYP method of density functional theory (DFT). For main group atoms O, Na, C and H, the 6-311+g(d,p) basis set was used. Frequency calculations at the same level of theory were also performed to identify all the stationary points as minima (zero imaginary frequencies). All the DFT calculations were performed with GAUSSIAN 09 software packages.

Synthesis of Sodium Phenoxide

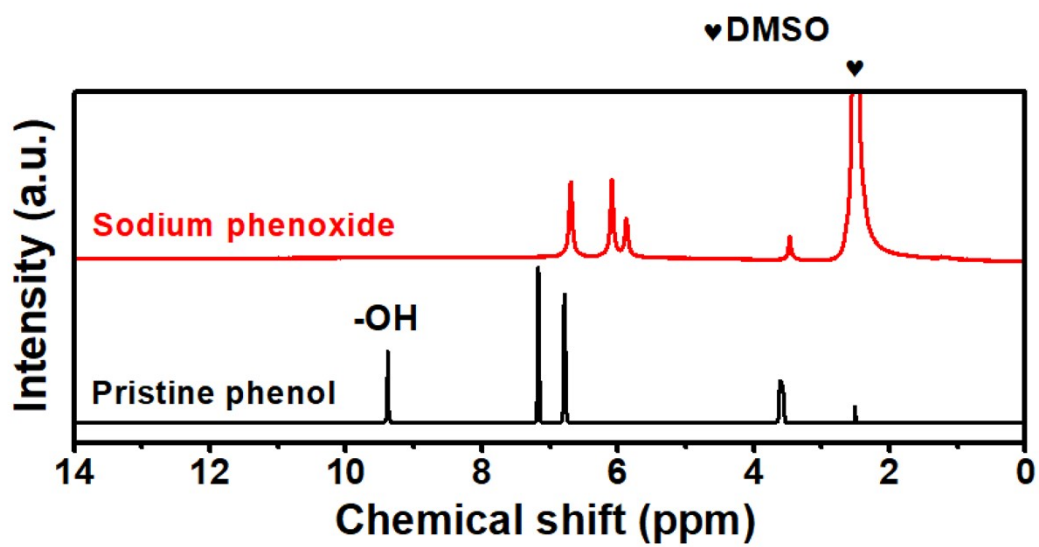


Figure S1: ¹H NMR spectra of synthesized sodium phenoxide in comparison to that of pristine phenol in DMSO-*d*₆.

Catalytic Hydrogenation of Sodium Phenoxide

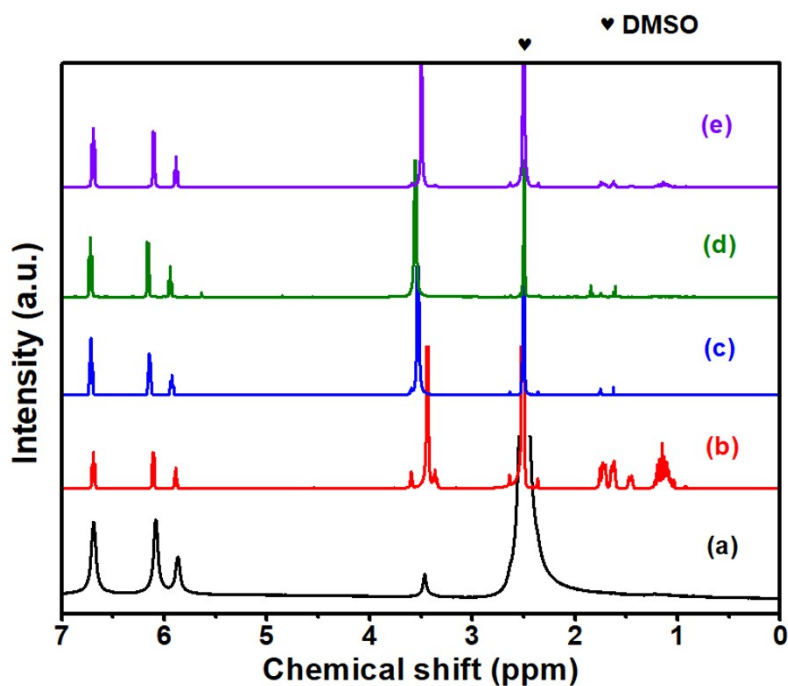


Figure S2: ^1H NMR spectra of the products obtained from room temperature hydrogenation of sodium phenoxide over different catalysts, (b) 5.0% Ru/TiO₂; (c) 5.0% Pd/TiO₂; (d) 5.0% Pt/TiO₂ and (e) 5.0% Ru/Al₂O₃, in DMSO-*d*₆. ^1H NMR spectrum of (a) sodium phenoxide was also included for comparison.

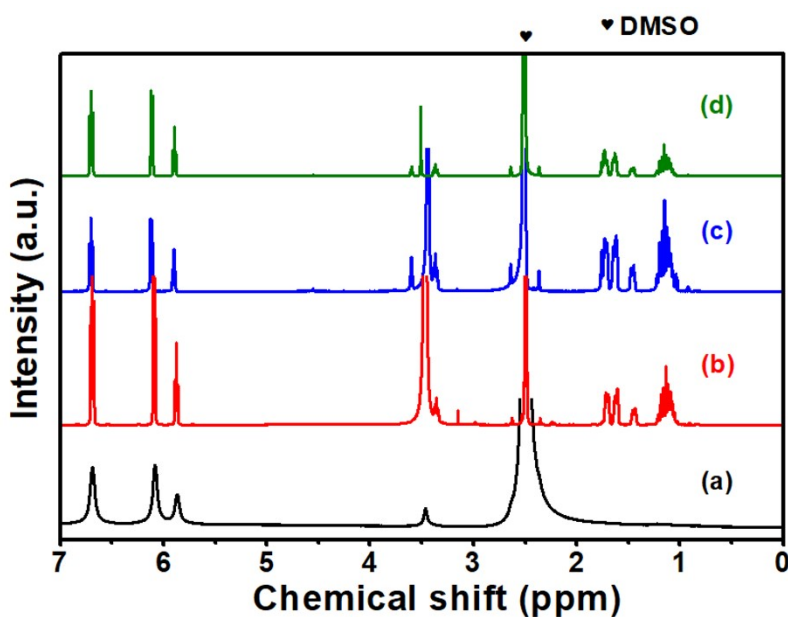


Figure S3: ^1H NMR spectra of the products obtained from hydrogenated sodium phenoxide over Ru/TiO₂ at different Ru loadings (b) 2.0% Ru/TiO₂; (c) 5.0% Ru/TiO₂; and (d) 9.7% Ru/TiO₂ in DMSO-*d*₆. ^1H NMR spectrum of (a) sodium phenoxide was also included for comparison.

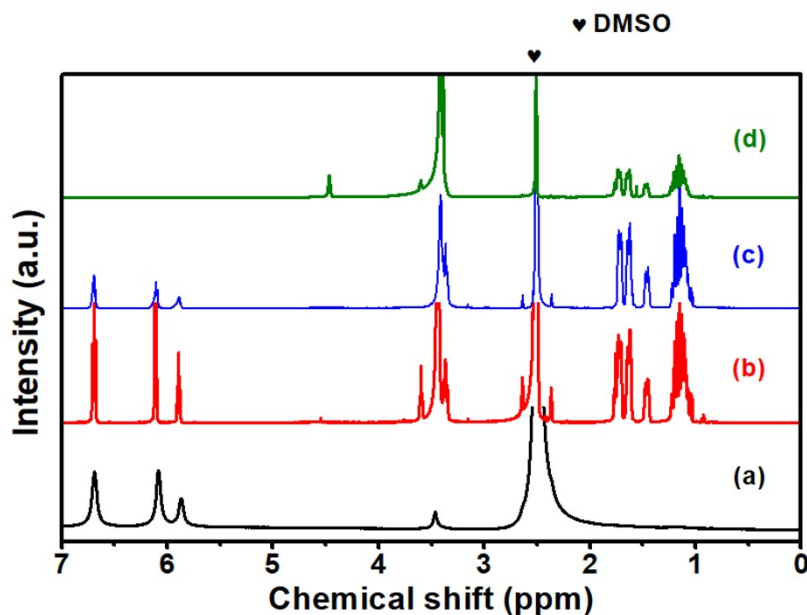


Figure S4: ^1H NMR spectra of the products obtained from hydrogenated sodium phenoxide over Ru/TiO_2 at different temperatures (b) room temperature; (c) $36\text{ }^\circ\text{C}$; and (d) $53\text{ }^\circ\text{C}$ in $\text{DMSO-}d_6$. ^1H NMR spectrum of (a) sodium phenoxide was also included for comparison.

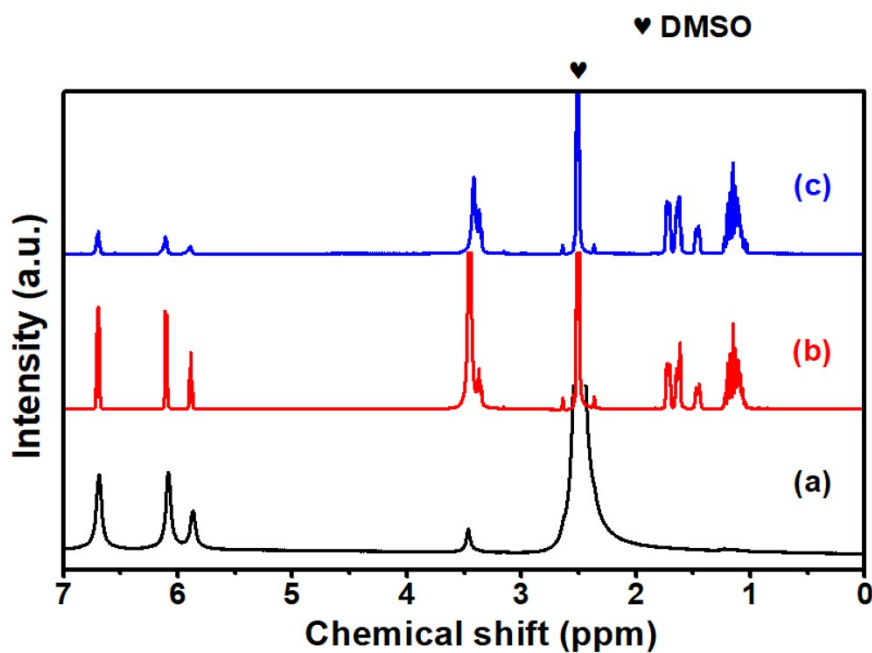


Figure S5: ^1H NMR spectra of the products obtained from hydrogenated sodium phenoxide over Ru/TiO_2 at different pressures (b) 5 bar and (c) 20 bar in $\text{DMSO-}d_6$. ^1H NMR spectrum of (a) sodium phenoxide was also included for comparison.

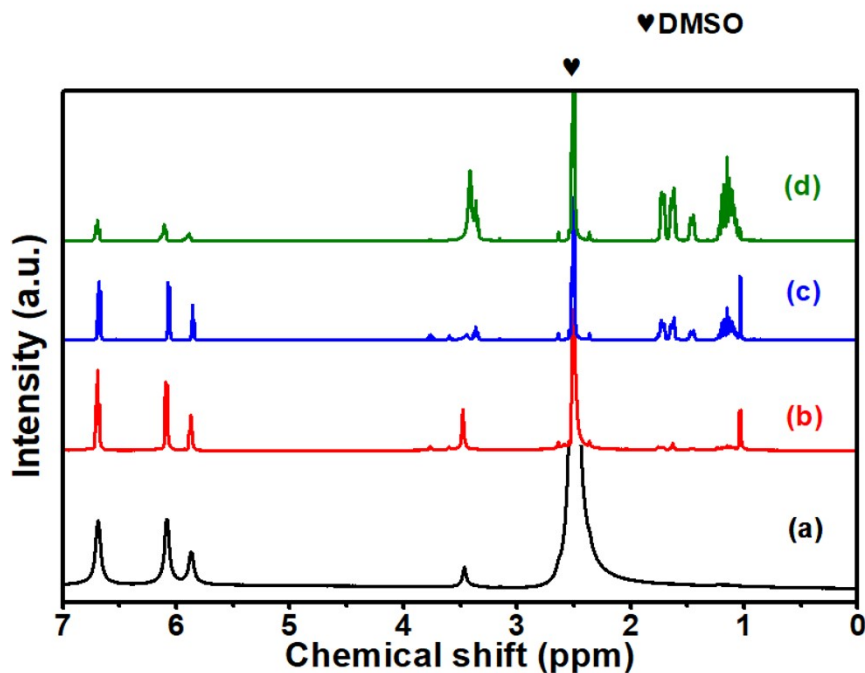


Figure S6: ¹H NMR spectra of the products obtained from hydrogenated sodium phenoxide over Ru/TiO₂ at 36 °C in different time intervals (b) 2 hours; (c) 5 hours; and (d) 20 hours in DMSO-*d*₆. ¹H NMR spectrum of (a) sodium phenoxide was also included for comparison.

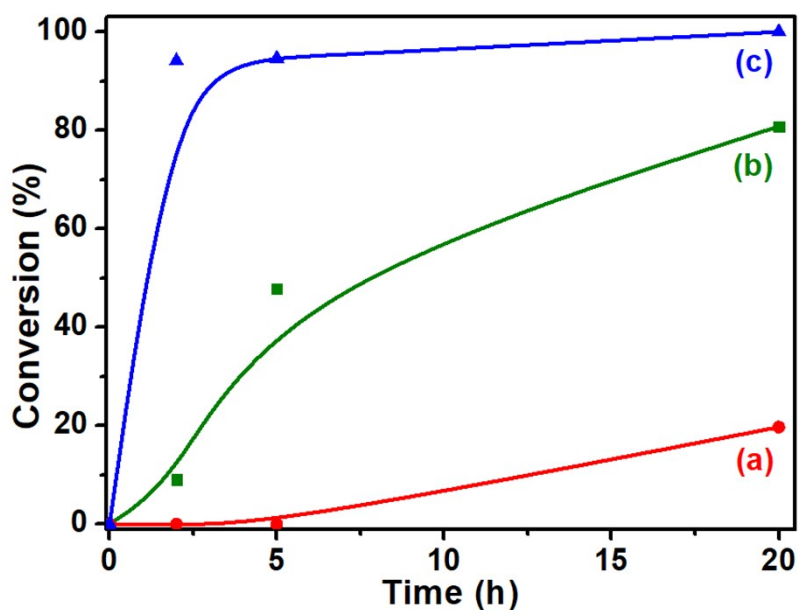


Figure S7: Catalytic hydrogenation of sodium phenoxide using (a) 5.0% Ru/Al₂O₃ at 36°C, (b) 5.0% Ru/TiO₂ at 36°C, and (c) 5.0% Ru/TiO₂ at 53°C, under 20 bar of H₂ pressure at different time intervals.

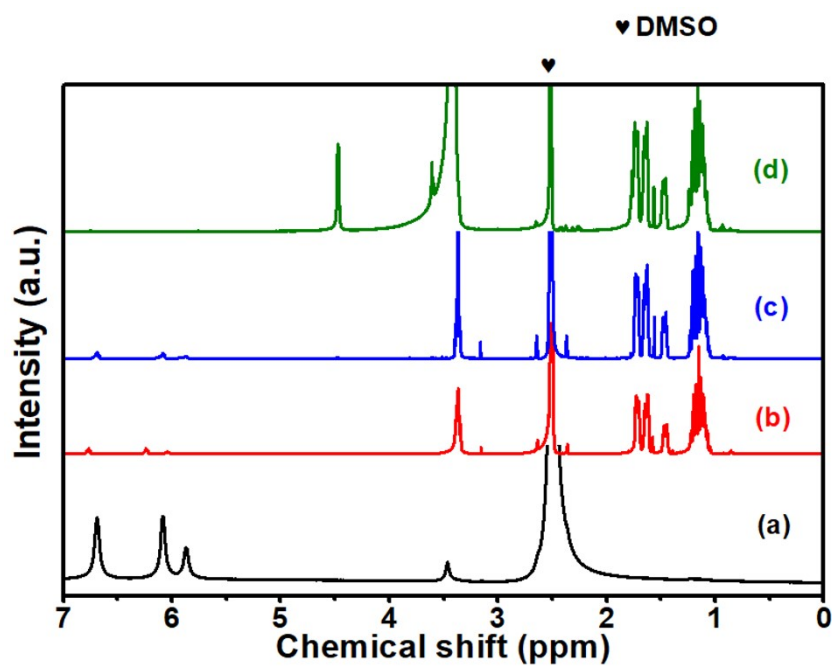


Figure S8: ^1H NMR spectra of the products obtained from hydrogenated sodium phenoxide over Ru/TiO_2 at $53\text{ }^\circ\text{C}$ in different time intervals (b) 2 hours; (c) 5 hours; and (d) 20 hours in $\text{DMSO-}d_6$. ^1H NMR spectrum of (a) sodium phenoxide was also included for comparison.

Catalysts Characterization

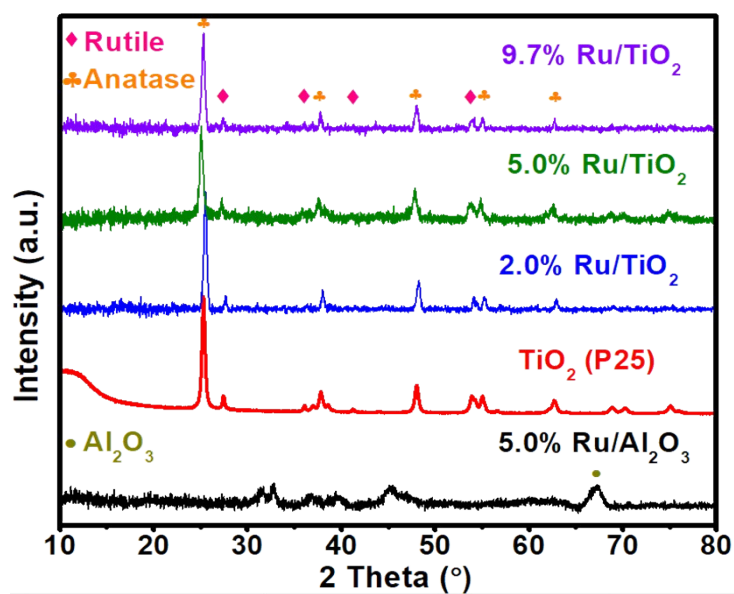


Figure S9: XRD patterns of the synthesized Ru/TiO₂ at different Ru loadings. The patterns of the commercial 5.0% Ru/Al₂O₃ and P25 TiO₂ were also included for comparison.

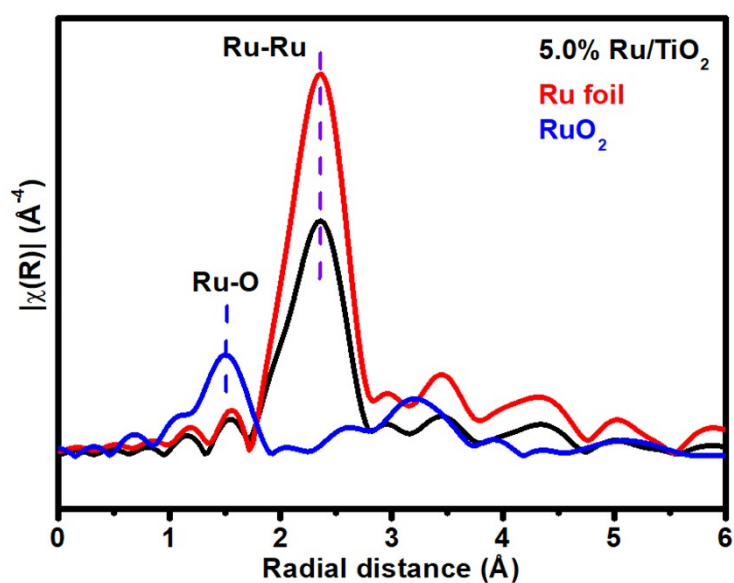


Figure S10: Fourier transforms of k^3 -weighted Ru K-edge EXAFS spectra.

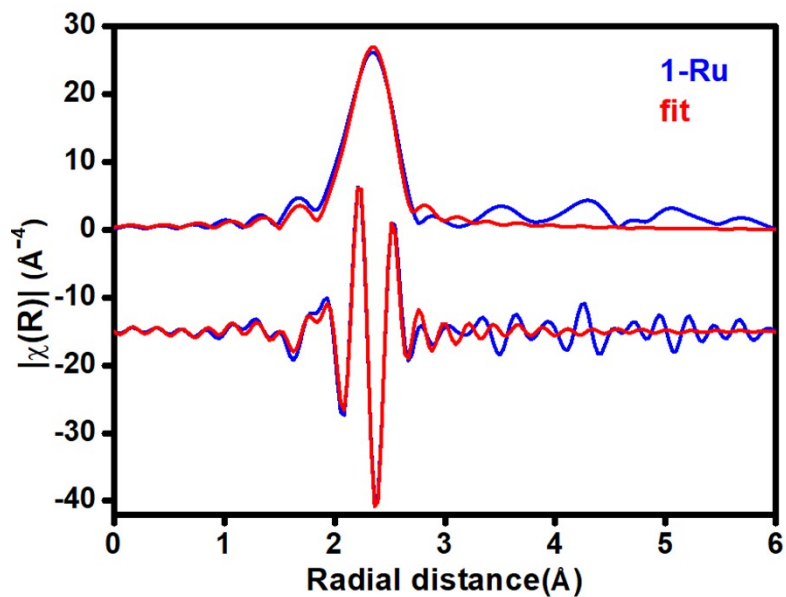


Figure S11: The fitting analysis for the as-synthesized 5.0% Ru/TiO₂ catalyst.

Table S1: EXAFS data fitting results of Ru foil and 5.0% Ru/TiO₂. D.W. stands for Debye-Waller and CN stands for coordination number.

Samples	Ru-Ru		D. W. (Å ²)	ΔE ₀ (eV)	R factor
	Distance (Å)	CN			
Ru foil	2.65±0.004	6.0±0.6	0.0028±0.0005	-5.1±0.8	0.015
	2.70±0.004	6.0±0.6			
5.0% Ru/TiO ₂	2.65±0.005	4.9±0.6	0.0042±0.0007	-6.3±1.0	0.025
	2.70±0.005	4.9±0.6			

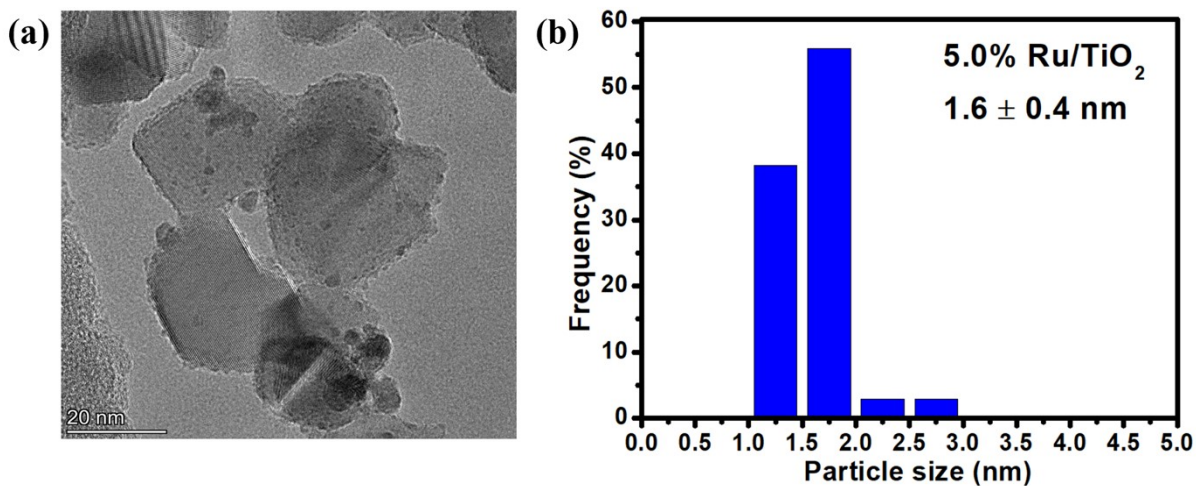


Figure S12: (a-b) TEM image and Ru particle size distribution of synthesized 5.0% Ru/TiO₂.

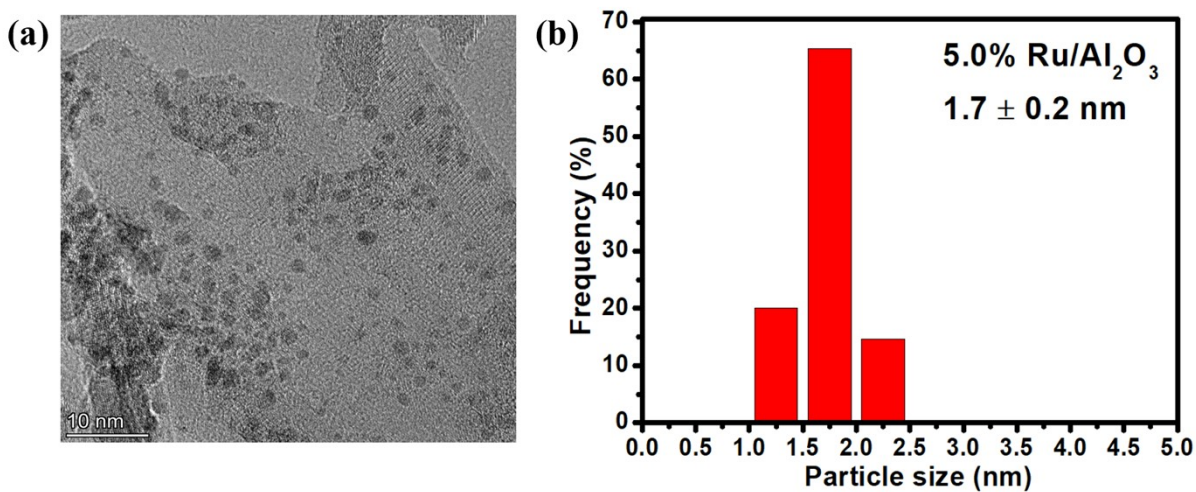


Figure S13: (a-b) TEM image and Ru particle size distribution of commercial 5.0% Ru/Al₂O₃.

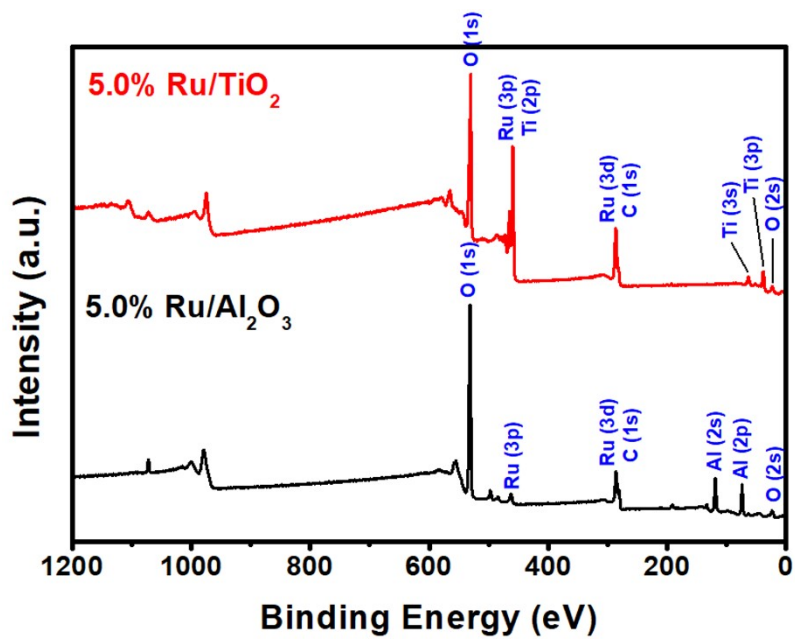


Figure S14: XPS spectra of full survey of 5.0% Ru/TiO₂ and 5.0% Ru/Al₂O₃.

Mechanism on the hydrogenation of sodium phenoxide over Ru/TiO₂ catalyst

Here, a plausible mechanism for the catalytic hydrogenation is proposed and is shown in Figure S15. It was reported that dihydrogen could be heterolytically split on the electron-rich metal surface^{4, 5}, forming H^{δ+} and H^{δ-} species on metal and support, respectively. Therefore, in the presence study, the molecular hydrogen could be readily activated at the Ru surface^{6, 7} and heterolytically split into H^{δ+} and H^{δ-} (**step 1**). When a phenoxide molecule approaches the catalyst surface, the molecule may lie on the interface region because of the electrostatic attraction. Then, H^{δ-} absorbed at the interface may attack the double bonds in phenol ring, followed by a H spillover from Ru surface to interface for further hydrogenation (**steps 2 and 3**). Our preliminary simulation found that sodium phenoxide complex **1** could easily isomerize to a cation- π adduct complex **2** configuration that has the sodium cation on the face of benzene ring with the energy barrier as low as 8.99 kcal/mol (Figure S16). In this cation- π adduct complex **2**, polar double bond C=O can be formed with the bond length of 1.245 Å. The polar C=O bond may be more susceptible to hydrogenation than the C=C bond in phenoxide ring due to the heterolytic H species (H^{δ+} and H^{δ-}) on the catalyst surface. Once the first double bond is broken, the aromaticity could be destroyed, facilitating the following hydrogenation. Therefore, by subsequent addition of 2 moles of hydrogen through heterolytic activation of the hydrogen molecule, a fully hydrogenated product, sodium cyclohexanolate, can be produced (**steps 4 and 5**).

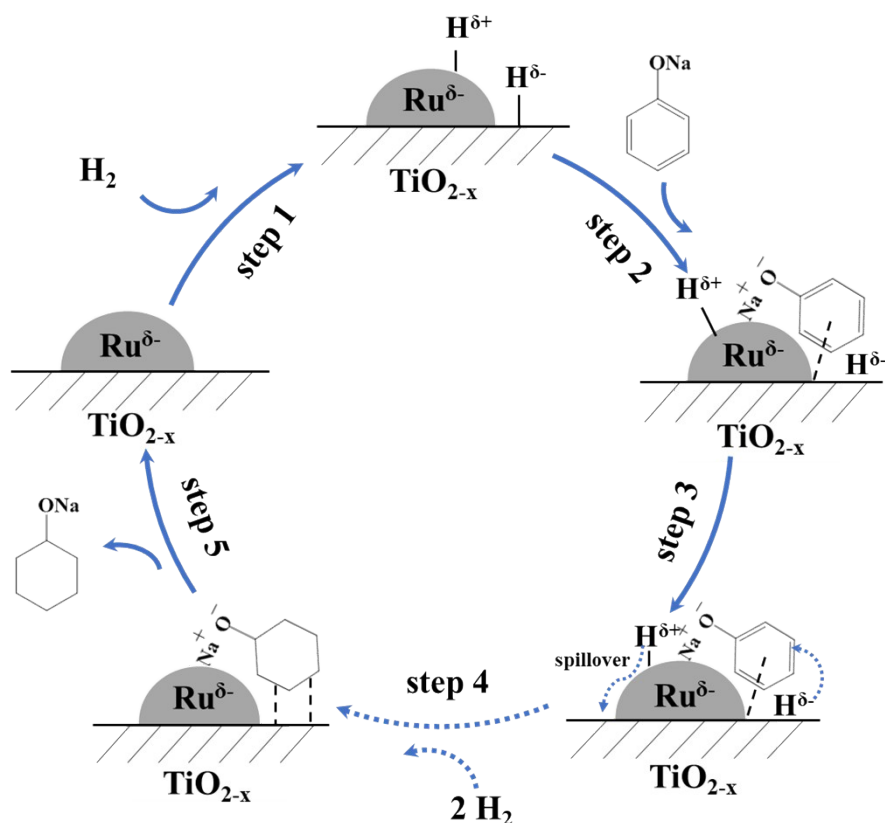


Figure S15: Schematic pathway describing the catalytic hydrogenation of sodium phenoxide over the ruthenium loaded on titania catalyst.

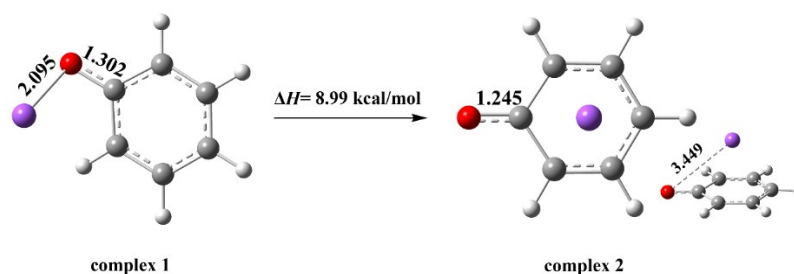


Figure S16: Optimization geometries parameters and enthalpy changes of sodium phenoxide complex **1** and cation- π adduct complex **2** systems. (The red, purple, gray and white spheres represent the O, Na, C and H atoms, respectively.)

References

1. Y. Yu, T. He, A. Wu, Q. Pei, A. Karkamkar, T. Autrey and P. Chen, *Angewandte Chemie*, 2019, **131**, 3134-3139.
2. H. Liu, G. Wei, Z. Xu, P. Liu and Y. Li, *Applied Surface Science*, 2016, **389**, 438-446.
3. B. Ravel and M. Newville, *J. Synchrotron Radiat.*, 2005, **12**, 537-541.
4. P. Liu, Y. Zhao, R. Qin, S. Mo, G. Chen, L. Gu, D. M. Chevrier, P. Zhang, Q. Guo, D. Zang, B. Wu, G. Fu and N. Zheng, *Science*, 2016, **352**, 797-800.
5. T.-N. Ye, J. Li, M. Kitano and H. Hosono, *Green Chemistry*, 2017, **19**, 749-756.
6. M. J. Gilkey and B. Xu, *ACS catalysis*, 2016, **6**, 1420-1436.

7. R. Qin, L. Zhou, P. Liu, Y. Gong, K. Liu, C. Xu, Y. Zhao, L. Gu, G. Fu and N. Zheng, *Nature Catalysis*, 2020, **3**, 703-709.